S©MR

СИБИРСКИЕ ЭЛЕКТРОННЫЕ
МАТЕМАТИЧЕСКИЕ ИЗВЕСТИЯ
Siberian Electronic Mathematical Reports
http://semr.math.nsc.ru
ISSN 1813-3304

Vol. 20, No. 2, pp. 144–145 (2023)
https://doi.org/10.33048/semi.2023.20.???
49N30

УДК 551.51, 519.68
MSC 76B60,

ROSSBY WAVE APPROXIMATION USING TWO-STRATEGY ADAPTIVE ARTIFICIAL BEE COLONY ALGORITHM

V.I. SIVTSEVA, **A.V. SAVVIN**, AND **V.V. GRIGORIEV**

Communicated by P.P. Petrov

Abstract: This paper presents an approach to approximating Rossby waves using the Two-Strategy adaptive Artificial Bee Colony (TSaABC) algorithm with hard thresholding. Rossby waves, as large-scale planetary waves, play a critical role in atmospheric dynamics, influencing meteorological phenomena and climate patterns. The study employs the TSaABC algorithm to optimize the parameters of a nonlinear space-time model representing atmospheric temperature data, drawn from the Aura (MLS) satellite. By solving the inverse problem involving minimizing the data discrepancy and L_1-norm of harmonic amplitudes, the method achieves a good accuracy and sparsity in the large dictionary of harmonics. To solve L_1-minimization, we design hard thresholding strategy within TSaABC. The implementation of hard thresholding allows for a reduction in dimensionality, which enhances computational efficiency. The results highlight the algorithm's potential for improving atmospheric modeling and forecasting.

Sivtseva, V.I., Savvin, A.V., Grigoriev, V.V., Rossby wave approximation using Two-Strategy adaptive Artificial Bee Colony algorithm.

The work is supported by the grant of Russian Science Foundation no. 23-71-30013(https://rscf.ru/project/23-71-30013/) and by Ministry of Education and Science of the Russian Federation under grant no. FSRG-2023-0025.

Received October, 10, 2024, Published December, 31, 2024.

Keywords: Atmospheric wave dynamics, Rossby waves, Artificial Bee Colony method, satellite data, Aura (MLS).

1 Introduction

The atmosphere can be considered as an ideal geophysical fluid that is permeated by waves of different spatial and temporal scales. Hydrodynamic quantities - wind, atmospheric gas component concentrations, pressure, density and temperature - experience periodic changes (oscillations). Different internal waves can be excited by different mechanisms, but in general, meteorological processes are the main sources of these motions. Gravity waves are able to propagate upward and grow in amplitude because of the exponentially decreasing neutral atmospheric density ρ (in order for the conservation laws of wave motion to be satisfied). Therefore, although the wave disturbances associated with small-scale (mesoscale) gravity waves are relatively small at source levels, their amplitudes can become significant at high altitudes in the upper mesosphere and thermosphere. On the other hand, large-scale waves such as planetary waves can have relatively large amplitudes in the lower atmosphere and hence can dissipate at lower altitudes. This wave dissipation is the mechanism for transferring momentum and energy from the disturbance to the mean flow. Mesoscale atmospheric waves can interact with other wave types and with the mean flow. For example, contribute to the generation or pumping of large-scale wave energy into smaller waves [1, 2, 3], and accelerate or decelerate the mean flow. A detailed study of these processes represents a crucial step toward a better understanding of the mechanisms of coupling between meteorology and space weather.

Various methods exist for detecting wave structures and processes in the atmosphere. These methods can be used to observe atmospheric temperature, pressure, wind fields, humidity, solar radiation flux, trace elements, electrical properties and precipitation. A variety of small and large-scale structures can be identified in the measured hydrodynamic fields that exhibit systematic wavelike changes and thus indicate wave propagation. As more technically sophisticated instruments with higher resolution are developed, the ability to detect finer structures increases. To date, the combination of ground-based observational techniques and satellite remote sensing provides an unprecedented view of the local and global state and composition of almost the entire Earth's atmosphere.

Metaheuristic algorithms are often used in studying different and distinct applications. Among metaheuristic methods, evolutionary and behavioral ones are commonly used. Behavioral methods are multi-agent methods based on modeling the intellectual behavior of agent colonies (swarm intelligence). Over the past few decades, swarm intelligence has drawn the attention of numerous researchers and practitioners. In the paper, we use the Artificial Bee Colony (ABC) method [4]. This algorithm is a swarm-based optimization

algorithm inspired by honey-bees behavior in nature. The following works [4, 5] contain more information on the algorithm's performance and convergence. This algorithm has proven itself in multidimensional optimization problems as being simple to implement, capable of parallelization and applicable to non-convex functionals. Since the introduction of this algorithm, many scientists have worked on improvements and modifications.

In this paper, we approximate temperature data using a sum of Rossby wave harmonics with unknown parameters that include amplitudes and wave numbers. We set the problem as an optimization problem, where the objective function is the sum of the data discrepancy function and the L_1-norm of harmonic amplitudes. The L_1-norm discrepancy is used to account for sparsity. This complex nonlinear space-time optimization problem is solved using Two-Strategy adaptive Artificial Bee Colony (TSaABC) optimization algorithm [6] with a modification that uses hard thresholding (HT). HT is used to adaptively reduce the parameter space dimension by eliminating the degrees of freedom that are negligible. This algorithm searches for best fit by varying the parameters in a systematic way. TSaABC in itself is a modification of the original ABC algorithm which adaptively uses two different strategies for evaluation and exploration of the functional space and has fast convergence compared to original ABC algorithm. HT improves the performance of TSaABC by reducing the parameter space, as our results show. Our results also show that we can achieve about 12% accuracy, which is considered to be a good accuracy given the presence of short-wave disturbances in the atmosphere, such as internal gravity waves.

Compared to our previous work (in press [7]), we use L_1 minimization and can explore a large number of harmonics where we can identify relevant harmonics. This is a significant improvement. Our methods also share some common concepts with instantaneous frequency approaches proposed in [8, 9]. In general, finding appropriate harmonics can greatly benefit in predicting atmospheric wave dynamics.

The paper is organized as follows. In the next section we give some preliminary information about planetary waves. Section 3 is devoted to the data used in the paper. The formulation of the inverse problem is given in Section 4. The peculiarities of the proposed algorithm are discussed in Section 5. The numerical results are presented in Section 6.

2 Planetary waves

The term «planetary waves» (PWs) refers to large-scale wave disturbances in the atmosphere with global dimensions. These waves can be generated by various sources, such as surface irregularities, temperature differences caused by uneven heating of land and sea, lunar gravitational tides, and large-scale meteorological events. During the winter season, the stratosphere and mesosphere are primarily dominated by Rossby waves, which arise due

to the balance between the latitudinal gradient of the Coriolis force and changes in the pressure gradient force [10, 11].

Planetary waves are considered to be an important driving mechanism of the meridional atmospheric circulation [12], which, due to its global character, determines the dynamic interaction of different layers and regions of the atmosphere. In addition, the overturning of planetary waves propagating from the troposphere upward can cause the development of sudden stratospheric warming in winter [13].

There are two types of PWs: stationary (or quasi-stationary) and traveling. Stationary PWs have long been known in the lower and middle layers of the atmosphere and demonstrate a pronounced seasonal character. Traveling PWs have a period from 2 to 30 days. They include the PWs propagating both eastward and westward. There are also zonal-symmetric waves, which we can consider as traveling PWs with zonal wave number zero (although, strictly speaking, they do not move).

Quasi-stationary Rossby waves are the dominant disturbances in the extra-tropical winter stratosphere and lower mesosphere. Rossby waves are excited by instabilities in the tropospheric jet stream: barotropic (due to horizontal wind shear) or baroclinic (due to vertical wind shear), respectively. They manifest themselves as sinuous jet streams, where the number of meanders (bends) gives the zonal wave number. Rossby waves are highly dispersive: those with higher velocities tend not to propagate vertically. Stationary Rossby waves with low zonal wave numbers (typically wave numbers 1-3) can propagate vertically, where the background averaged zonal wind is westerly [14]. This condition is usually fulfilled in the winter stratosphere and lower mesosphere. The winter zonal wind can change from westerly to easterly in the upper mesosphere; the height at which the wind reversal occurs varies with latitude, season, and can have large interannual variations due to dynamical activity. Quasi-stationary waves are difficult to separate from wind and temperature backgrounds in radar and lidar observations, but can be observed from satellites. In Mukhtarov et al. (2010) [15] present observations of stationary temperature waves observed by the SABER satellite instrument. Quasi-stationary planetary waves have been observed in the winter mesosphere–lower thermosphere (MLT) [16, 17].

Planetary-scale traveling waves can reach large amplitudes in the MLT. The periods of traveling waves are clustered around periods associated with normal atmospheric modes. One frequently observed mode is a quasi-two-day wave with a period of about 2 days and a zonal wave number of 3 or 4. Quasi-two-day waves are regularly observed in the mesosphere just after solstices and can reach very large amplitudes (meridional wind 30 m/s) [18]. Other commonly recorded periods: 5 days, 6.5 days, 10 and 16 days. These waves do not directly carry a large momentum. However, they can interact with other waves such as quasi-stationary Rossby waves, gravity waves, and tides, and thus affect the momentum balance and periodicity of

variability in the middle atmosphere. A spectral analysis of planetary waves in mesospheric observations has been given by Garcia et al. [19].

For the mathematical description of Rossby waves [20] we set the total horizontal wind field (u, v), where u and v are the wind components in the x and y directions, respectively (coordinate x is oriented eastward, y is oriented northward). The total wind field can be written as the mean flow U with a small superimposed perturbation u' and v'

$$u = U + u'(t, x, y),$$
$$v = v'(t, x, y).$$

The perturbation is assumed to be much smaller than the mean zonal flow $U \gg u', v'$.

The relative curl and perturbations can be written through the stream function ψ (provided the flow is not divergent, for which the flow function fully describes the flow):

$$\begin{aligned} u' &= \frac{\partial \psi}{\partial y}, \\ v' &= -\frac{\partial \psi}{\partial x}, \\ \eta &= \nabla \times (u'\,\widehat{\imath} + v'\,\widehat{\jmath}) = -\nabla^2 \psi. \end{aligned} \tag{1}$$

According to the work of Carl Rossby [21], the large-scale structure of a two-dimensional non-divergent barotropic flow can be modeled under the assumption that the relative vorticity η is conserved.

$$\frac{d(\eta + f)}{dt} = 0,$$

where f is the Coriolis force, which is equal to $f = 2\Omega sin\varphi$. Ω and φ are the earth's angular velocity and latitude on the earth, respectively. If the coordinate y is measured from a reference latitude φ_0 then $\varphi = \varphi_0 + y/a$, where a is the earth's radius (6371 km).

In the β-plane approximation ($f \approx f_0 + \beta y$, $\beta = \frac{\partial f}{\partial y} = \frac{1}{a}\frac{\mathrm{d}}{\mathrm{d}\varphi} 2\Omega sin\varphi = \frac{2\Omega cos\varphi}{a}$), we obtain the following expression

$$\frac{\partial \eta}{\partial t} + U\frac{\partial \eta}{\partial x} + \beta v' = 0.$$

We then substitute the definition of the stream function (1) to get the following equation

$$\frac{\partial \nabla^2 \psi}{\partial t} + U\frac{\partial \nabla^2 \psi}{\partial x} + \beta \frac{\partial \psi}{\partial x} = 0. \tag{2}$$

We consider a plane wave solution with zonal and meridional wave numbers k and l, respectively, and frequency ω

$$\psi(t, x, y) = A\, exp\, \imath(kx + ly - \omega t). \tag{3}$$

Then, substituting the plane wave equation into the original expression (2), we obtain the relation for the frequency ω

$$\omega = uk + \beta \frac{k}{k^2 + l^2}.$$

3 Data Sets

Data from the Aura satellite are used in this work. In particular, data from the EOS MLS instrument. Aura is a research satellite designed to study the Earth's atmosphere [22]. The satellite was launched into a sun-synchronous orbit on July 15, 2004 at an altitude of 705 km. Aura makes about 15 passes per day with a period of ∼100 min

Atmospheric temperature measurements obtained by the Microwave Limb Sounder (MLS) on the Aura satellite, Level 2, version 4.2x (*daac.gsfc.nasa.gov*), were used for the analysis. Approximately 3500 vertical profiles are measured by the Aura MLS system per day, covering a latitudinal range from 82°S to 82°N. Vertical profiles are measured at ∼25 s intervals every 1.5° (∼165 km) along the orbital trajectory. The MLS microwave probe scans the Earth limb in the flight direction, recording microwave emission in five spectrum bands (118 GHz, 190 GHz, 240 GHz, 640 GHz, 2.5 THz). The instrument measures the temperature and chemical composition of the atmosphere at 55 pressure levels from 1000 to 10-5 hPa (0-130 km) [23]. The geopotential height is calculated from the integration of the hydrostatic equation above a reference level of 100 hPa. The working region for scientific studies is the 261-0.001 hPa height interval (∼10-92 km, 42 levels/layer). The vertical resolution of the data is about 5 km around the MLT. Temperature measurement accuracy is $\sim \pm 1$ K in the 10-80 km altitude interval and $\sim \pm 2.3$ K in the 80-92 km interval. Below 10 km and above 92 km, the measurement errors increase significantly [24]. Raw data files in HDF-EOS format (hierarchical data format) are available at the *acdisc.gesdisc.eosdis.nasa.gov*.

MLS observations at a given latitude on the ascending or descending sides of the orbit have approximately the same local solar time (to within a few minutes) throughout the mission. Consequently, the temperature data of the MLS (Aura) probe can be considered without taking into account the contribution of tidal waves, since the tides are mainly due to the change of day and night (moving of the day-night terminator). At latitude 63°N the satellite takes readings once per night at about the same local solar time (∼03:00).

Since the Rossby waves have a zonal structure, temperature data falling on the latitudinal ring from 58°N to 68°N were selected for approximation. To exclude a large contribution of diurnal temperature variations, night data were sampled. Overnight sample data is presented in Figure 1. The figure illustrates the distribution of temperature measurements taken by the Aura (MLS) across different longitudes (x-axis), latitudes (y-axis), and time (z-axis represents time (t) in second). There are 105 individual measurements,

distributed as follows: 7 measurements along the latitude axis and 15 measurements along the longitude axis.

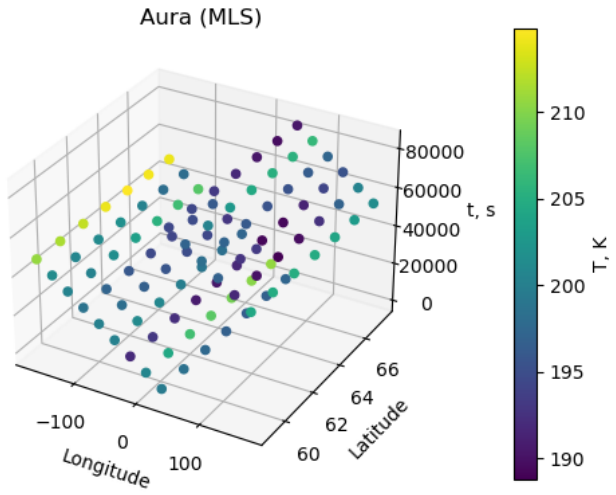

FIG. 1. Nocturnal measurements of EOS MLS (06 March 2011) at latitude 58-68°N at an altitude ∼80 km.

4 Inverse problem formulation

In this study, PWs are analyzed similar to the method presented in Preusse et al. [25, 26] and Fetzer and Gillet [27]. Our proposed method is summarized as follows. The temperature components corresponding to zonal wave numbers are estimated by an approximation function. For measurements at fixed local solar time, the contributions of all tidal components are included in the contributions of the components corresponding to wave numbers. Small-scale waves having large wave numbers belong to internal gravitational waves (IGW) and are not described by the Rossby wave equation. Consequently, the "background temperatures"(T_{bg}) are estimated by the above method must contain the zonal mean temperature (T_{zm}), planetary waves (T_{pw}) and tidal waves. Residual temperature perturbations (T_{gw}) (i.e., $T_{gw} = T_{Aura} - T_{bg}$, where T_{Aura} is measured temperatures), are considered as fluctuations caused by IGW.

The data is approximated by linear combination of harmonics from the dictionary $\{R_1, ..., R_m\}$. It is necessary to minimize the error using the smallest number of harmonics. One of the advantages of this approach is the possibility to use many different sets of harmonics in the dictionary. In our case each harmonic R_n in the dictionary is based on the Rossby wave

equation (the real part of the equation is considered) (3)

$$\begin{aligned} f_n &= k_n x + l_n y - (uk_n + \beta \frac{k_n}{k_n^2 + l_n^2})t, \\ R_n &= A_n \, cos \, (f_n), \end{aligned} \tag{4}$$

where k and n vary from 0 to m.

Equations (4) are used to construct the approximating function as the sum of Rossby waves in the following way

$$g = \sum_{n=1}^{m} R_n + C,$$

where C is a constant. The relative error of temperature variations is minimized: the ratio of the L_2-norm of the absolute approximation error to the L_2-norm of temperature variations

$$\varepsilon_{rel} = \frac{\|g - T_{Aura}\|_2}{\|T_{Aura} - C\|_2}.$$

Also, to minimize the count of harmonics the weighted L_1-norm of the amplitude coefficients $(A_1, ..., A_m)$ is used

$$\|A\|_1 = \sum_{n=1}^{m} \omega_n |A_n|.$$

The weights are selected such that

$$w_1 < w_2 < \cdots < w_m,$$

where m is the harmonic number and weights are chosen within the range $(0, 1]$ and are distributed exponentially. Therefore, the shortest-wave harmonic has a greater chance of being zeroed out. The higher is the weight, the smaller is the amplitude, and thus the greater is the chance of being rejected.

The objective function is the sum of the relative error and L_1-norm from the amplitude coefficients $(A_1, ..., A_m)$

$$\mathcal{F}(\vartheta) = \varepsilon_{rel} + \gamma \, \|A\|_1 \, , \tag{5}$$

where ϑ is a vector of our coefficients, γ is a parameter that brings the terms of the objective function into a single order so that none of them becomes dominant. Thus, our inverse problem reduces to the problem of identification of the key parameters defining the Rossby waves, which is viewed as a problem of minimizing the objective function given above.

5 Two-Strategy adaptive Artificial Bee Colony algorithm with hard thresholding

The Artificial Bee Colony (ABC) algorithm has always struggled with how to dynamically modify exploration and exploitation during the process of evolution. For this work we will exploit the Two-Strategy adaptive Artificial

Bee Colony (TSaABC) optimization algorithm, which is presented by Xiaoyu Song et. al [6]. This algorithm is a combination of two different modification of ABC algorithm (CABC with CABC_Elite [28] and M2ABC [29]) and overcome described above issues of the classic algorithm. The TSaABS algorithm adaptively chooses two different search strategies based on the relations of the success rates of candidate solution inspired by work [30]. The performance and comparison analysis with detailed pseudocode of the algorithm can be seen in [6].

We will not describe the algorithm in details, but will simply highlight the key points:

1. Initialization
   - The position of the food source in the algorithm indicates a potential solution of the optimization problem, and the amount of nectar in the food source indicates the suitability (fitness) of the corresponding solution. The number of bees is equal to the number of solutions in the population. At the first step (initialization):

$$\vartheta_{i,j} = \vartheta_{i,j}^{min} + \phi(\vartheta_{i,j}^{max} - \vartheta_{i,j}^{min}), \tag{6}$$

     generates a randomly distributed initial population of SN solutions (food source positions), where SN denotes the bees count and therefore the number of solutions, ϕ is randomly generated number between [0, 1]. Here $\vartheta_{i,j}$ is a bee object where indices are following: $i = 1, 2, ..., SN$, $j = 1, 2, ..., D$ is the number of optimization parameters. Also $\vartheta_{i,j}^{max}$ and $\vartheta_{i,j}^{min}$ is a upper and lower bounds of each optimized parameter respectively. Therefore, each bee has a starting point located inside searching area.
   - After initialization, the process of searching for the best nectar begins, which occurs in cycles $cn = 1, \ldots, MCN$ (maximum cycle number).
2. Applying Adaptive Strategy Selection
   - Each employed bee applies one of the two strategies (CABC or M2ABC) to update its solution. To dynamically select between the two strategies, an adaptive mechanism is used. The probability ξ_{cn} for selecting a strategy is updated based on the success rate of solutions from previous generations:

$$\xi_{cn+1} = \alpha \cdot \xi_{cn} + (1 - \alpha) \cdot P_{cn},$$

     where $P_{cn} = S_{cn}^1/(S_{cn}^1 + S_{cn}^2)$ is the success rate of strategy 1 relative to strategy 2 in the previous generation, and S_{cn}^q represents the number of successful solution updates by strategy q and real number $\alpha \in [0, 1]$ is used to control the proportion of historical experience and in this work set as 0.95, $\xi_1 = 0.5$.
     - *Strategy 1*: CABC. To maintain exploration capabilities, the first strategy (CABC) generates new candidate solutions based on

random directions. The update equation is:

$$\widehat{\vartheta}_{i,j} = \vartheta_{r1,j} + \varphi(\vartheta_{r1,j} - \vartheta_{r2,j}), \tag{7}$$

where at this stage j, $r1$ and $r2$ is randomly selected and $r1, r2 \in \{1, 2, \ldots, SN\}$, $j \in \{1, 2, \ldots, D\}$, $r1 \neq r2 \neq i$; φ is a uniform random number on [-1, 1]. In (7), the bees are randomly selected from the population and thus the equation has strong exploration ability and can go to any search direction.

– *Strategy 2*: M2ABC. To enhance exploitation, the second strategy uses information from the best solution found so far. The update equation is:

$$\widehat{\vartheta}_{i,j} = \frac{\vartheta_{r1,j} + \vartheta_{r2,j}}{2} + \phi_{i,j}(\vartheta_{r1,j} - \vartheta_{r2,j}) + \varphi_{i,j}(\vartheta_{best,j} - \vartheta_{r1,j}),$$

where $r1 \neq r2 \neq best$, $\vartheta_{best,j}$ is the j-th element of the best so far solution.

- *Strategy 2* will be used if random number between (0,1) $< \xi_{cn}$, *strategy 1* otherwise. The algorithm repeats from this step to 4-th until the maximum number of iterations is reached.

3. Solution Improvement and Update
   - Onlooker bees select the best solutions found by the employed bees and further improve them, using either strategy with probabilities ξ_{cn+1} and $1 - \xi_{cn+1}$. To ensure that each search strategy can be selected, ξ_{cn+1} is limited between $[0.1, 0.9]$.
   - If a new candidate solution $\widehat{\vartheta}_{i,j}$ is better than the current one $\vartheta_{i,j}$, it replaces the old solution, otherwise parameter $trial_i$ is increased by 1. If a solution has not been improved after $limit$ iterations ($trial_i = limit$), the corresponding bee becomes a scout via (6), abandoning its current solution and randomly generating a new one.
4. Hard Thresholding and Dimension Reduction
   - We assume a modification to TSaABC algorithm by adding hard thresholding (HT). The idea behind this approach is that during the optimization process we reduce the dimensionality of the problem by removing unnecessary harmonics:

$$R_n(A_n, \cdot) = \begin{cases} R_n(A_n, \cdot), & |A_n| \geq h, \\ 0, & |A_n| < h, \end{cases}$$

   where h is the threshold value.
   - Since we are trying to optimize a large number of harmonics, this approach is important, because in the conventional approach, it is not always possible to find an optimal solution due to very large parameter space. We use two rules that will ensure the adequacy of the algorithm in rejecting unnecessary harmonics:
     – HT only works after $\varkappa$ iterations. This allows the parameters to stabilize;

– HT is applied only if the value of the corresponding parameter does not increase during ζ iterations.

According to this approach, the solution of a multi-parameter optimization problem becomes computationally cheaper, and it is feasible to compute due to the dimensionality reduction.

6 Numerical experiment

To find the numerical solution, the parameters of the algorithm are set as follows: SN=100, MCN=2500, m=20, D=2*(m+1)+2=44, h=1 K, $\varkappa$=100, ζ=150. The other parameters of the algorithm are consistent with the work [6]. The threshold value h is set to 1 K because the measurement error is equal to 1 K (see Section 3).

TABLE 1. Boundaries ($\vartheta_{i,j}^{max}$ and $\vartheta_{i,j}^{min}$) of coefficient search.

Parameters	Lower	Upper
A_n, K	0	20
l_n	0	4
u, rad/s	-20/6371000	200/6371000
C, K	-20	20

Table 1 presents the boundaries ($\vartheta_{i,j}^{max}$ and $\vartheta_{i,j}^{min}$) of coefficient search for various parameters involved in the Rossby wave approximation. These parameters include mean zonal flow u in radians per second, meridional wavenumbers l for different harmonics, amplitude A in K, and a constant C also in K. The harmonic number n (4) ranges from 1 to m. The table lists these parameters, showing their respective values.

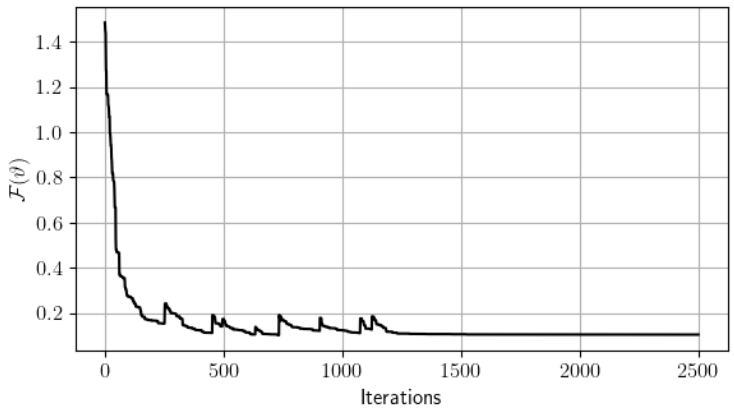

FIG. 2. Iterative history of objective function $\mathcal{F}(\vartheta)$.

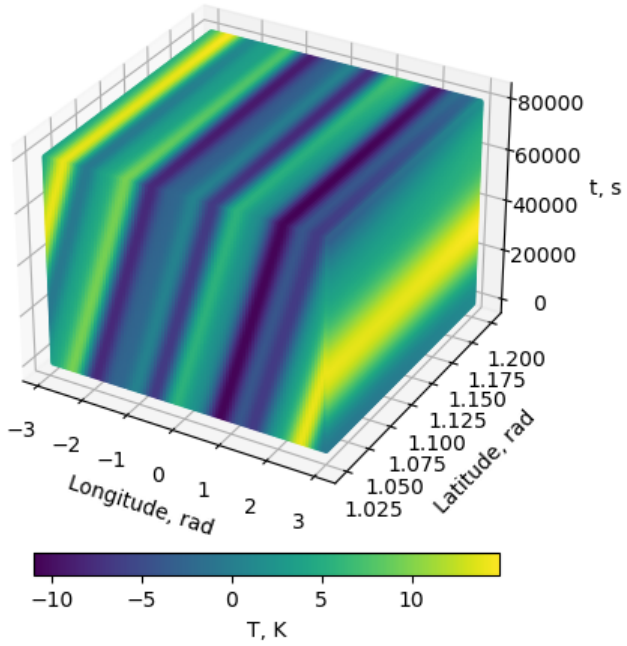

FIG. 3. Visualization of the approximation by the function g_{MCN}.

TABLE 2. Approximation results.

n	0	1	2	3	4	5	9
l_n	2.906	3.124	0.579	0.0	4.0	0.0	2.102
A_n, K	20.0	4.068	4.41	3.016	2.054	4.139	1.98
u, rad/s	1.635e-05						
C, K	20.0						
$\mathcal{F}(\vartheta)$	0.12						

The Figure 2 shows iterative history of objective function $\mathcal{F}(\vartheta)$ (5). The value of the objective function decreases to 0.12. The discrete jumps of the $\mathcal{F}$ value correspond to iterations when we remove some of the harmonics due to hard thresholding (see Section 5 (4)). The error of about 12% is reasonable, since there are short-wave disturbances in the atmosphere corresponding to, for example, IGW. Moreover, we observe that the method has converged as the error stabilizes. The approximation results are presented in Table 2

Figure 3 illustrates the three-dimensional representations of Rossby wave approximation for g_{MCN} function at an altitude of 80 km. The pattern shows the spatial and temporal distribution of the temperature variation T in K. The x-axis represents the longitude in radians, the y-axis represents the

latitude in radians, and the z-axis represents time in seconds. With this figure, we illustrate Rossby waves in space and time.

7 Conclusions

In this study, we propose a novel approximation for temperature data using L1-minimization with a dictionary of Rossby waves. Our proposed minimization employs the Two-Strategy adaptive Artificial Bee Colony (TSaABC) algorithm with hard thresholding strategy to solve this challenging optimization problem. Hard thresholding within TSaABC reduces the parameter space and makes the computation feasible. Our approach has been effective in reducing the dimensionality of the problem while maintaining accuracy, achieving good precision and sparsity.

The adaptive nature of the TSaABC algorithm allowed for dynamic exploration and exploitation, enabling it to handle the nonlinear and complex characteristics of atmospheric wave data. By minimizing the error and optimizing wave-number parameters, our method offers a reliable tool for atmospheric modeling, especially in approximating planetary-scale waves. Future work should focus on further refining the model by incorporating additional atmospheric variables and extending the algorithm to three-dimensional simulations. Moreover, testing the model under different atmospheric conditions will be essential to validate its robustness and reliability. Overall, the integration of TSaABC optimization with atmospheric wave dynamics represents a promising avenue for advancing meteorological research and improving predictive models.

References

[1] R. D. Lindzen, *Planetary waves on beta-planes*, Monthly Weather Review, **95**:7, (1967), 441-451.

[2] R. S. Lindzen, *Turbulence and stress owing to gravity wave and tidal breakdown*, Journal of Geophysical Research: Oceans, **86**:C10, (1981), 9707-9714.

[3] A. K. Smith, *Longitudinal Variations in Mesospheric Winds: Evidence for Gravity Wave Filtering by Planetary Waves*, Journal of the Atmospheric Sciences, **53**:8, (1996), 1156-1173.

[4] D. Karaboga, B. Basturk, *On the performance of artificial bee colony (ABC) algorithm*, Applied soft computing, **8**:1, (2008), 687–697.

[5] D. Karaboga, B. Akay, *A comparative study of artificial bee colony algorithm*, Applied mathematics and computation, **214**:1, (2009), 108–132.

[6] X. Song, M. Zhao, Q. Yan, S. Xing, *A high-efficiency adaptive artificial bee colony algorithm using two strategies for continuous optimization*, Swarm and Evolutionary Computation, **50**, (2019), 100549.

[7] V. I. Sivtseva and V. V. Grigoriev, *Temperature Data Approximation Using Rossby Waves*, Lobachevskii Journal of Mathematics, **45**:11, (2024), 5302–5311.

[8] T. Y. Hou and Z. Shi *Sparse Time-Frequency decomposition for multiple signals with same frequencies* Advances in Data Science and Adaptive Analysis, **9**:04, (2017), 1750010.

[9] N. E. Huang, Zh. Shen, S. R. Long, M. C. Wu, H. H. Shih, Q. Zheng, Nai-Chyuan Yen, Chi Chao Tung and H. H. Liu *The empirical mode decomposition and the Hilbert*

spectrum for nonlinear and non-stationary time series analysis, Proceedings of the Royal Society of London. Series A: mathematical, physical and engineering sciences, **454**:1971, (1998), 903-995.

[10] A. K. Smith, *Global Dynamics of the MLT*, Surveys in Geophysics, **33**:6, (2012), 1177-1230.

[11] E. Yigit and A. S. Medvedev, *Internal wave coupling processes in Earth's atmosphere*, Advances in Space Research, **33**:4, (2015), 983-1003.

[12] J. R. Holton, P. H. Haynes, M. E. McIntyre, A. R. Douglass, R. B. Rood, L. Pfister, *Stratosphere-troposphere exchange*, Reviews of Geophysics, **33**:4, (1995), 403-439.

[13] M. R. Schoeberl, *Stratospheric warmings: Observations and theory* Reviews of Geophysics, **16**:4, (1978), 521-538.

[14] J. G. Charney and P. G. Drazin, *Propagation of planetary-scale disturbances from the lower into the upper atmosphere* Journal of Geophysical Research, **66**:1, (1961), 83-109.

[15] P. Mukhtarov, D. Pancheva, and B. Andonov, *Climatology of the stationary planetary waves seen in the SABER/TIMED temperatures (2002-2007)* Journal of Geophysical Research, **115**, (2010), 2009JA015156.

[16] C. Xiao, X. Hu, and J. Tian, *Global temperature stationary planetary waves extending from 20 to 120 km observed by TIMED/SABER* Journal of Geophysical Research: Atmospheres, **114**, (2009), 2008JD011349.

[17] V. Sivtseva, P. Ammosov, G. Gavrilieva, A. Ammosova, I. Koltovskoi, *Wave activity of the mesosphere in the planetary wave range according to OH (3-1) emission observations at Maimaga and Tiksi stations for 2015-2020* Solar-Terrestrial Physics, **8**:4, (2022), 89-94.

[18] D. Offermann, P. Hoffmann, P. Knieling, R. Koppmann, J. Oberheide, D. M. Riggin, V. M. Tunbridge, and W. Steinbrecht, *Quasi 2 day waves in the summer mesosphere: Triple structure of amplitudes and long-term development* Journal of Geophysical Research, **116**, (2011), D00P02.

[19] R. R. Garcia, R. Lieberman, J. M. Russell, and M. G. Mlynczak, *Large-scale waves in the mesosphere and lower thermosphere observed by SABER* Journal of the Atmospheric Sciences, **62**:12, (2005), 4384-4399.

[20] R. E. Dickinson, *Rossby waves – long-period oscillations of oceans and atmospheres* Annual Review of Fluid Mechanics, **10**:1, (1978), 159-195.

[21] C. G. Rossby, *Planetary flow patterns in the atmosphere* Quarterly Journal of the Royal Meteorological Society, **66**, (1940), 68-87.

[22] M. R. Schoeberl, A. R. Douglass, E. Hilsenrath, P. K. Bhartia, R. Beer, J. W. Waters, M. R. Gunson, L. Froidevaux, J. C. Gille, J. J. Barnett, P. F. Levelt, and P. DeCola, *Overview of the EOS Aura mission* IEEE Transactions on Geoscience and Remote Sensing, **44**:5, (2006), 1066-1074.

[23] J. W. Waters et al., *The earth observing system microwave limb sounder (EOS MLS) on the Aura satellite* IEEE Transactions on Geoscience and Remote Sensing, **44**:5, (2006), 1075-1092.

[24] M. J. Schwartz et al., *Validation of the aura microwave limb sounder temperature and geopotential height measurements* Journal of Geophysical Research, **113**, (2008), D15S11.

[25] P. Preusse, A. Dornbrack, S. D. Eckermann, M. Riese, B. Schaeler, J. T. Bacmeister, D. Broutman, and K. U. Grossmann, *Space-based measurements of stratospheric mountain waves by CRISTA 1. sensitivity, analysis method, and a case study* Journal of Geophysical Research: Atmospheres, **107**, (2002), CRI6-1–CRI6-23.

[26] P. Preusse, S. D. Eckermann, M. Ern, J. Oberheide, R. H. Picard, R. G. Roble, M. Riese, J. M. Russell, and M. G. Mlynczak, *Global ray tracing simulations of the SABER gravity wave climatology* Journal of Geophysical Research, **114**, (2009), D08126.

[27] E. J. Fetzer and J. C. Gille, *Gravity wave variance in LIMS temperatures. Part I: Variability and comparison with background winds* Journal of the Atmospheric Sciences, **51**:17, (1994), 2461-2483.

[28] W. F. Gao, S. Y. Liu, L. L. Huang, *A novel artificial bee colony algorithm based on modified search equation and orthogonal learning*, IEEE Transactions on Cybernetics, **43**:3, (2013), 1011-1024.

[29] M. Črepinšek, S. H. Liu, M. Mernik, *Exploration and exploitation in evolutionary algorithms: A survey*, ACM computing surveys (CSUR), **45**:3, (2013), 1-33.

[30] J. L. Deneubourg, S. Aron, S. Goss, J. M. Pasteels, *The self-organizing exploratory pattern of the argentine ant*, Journal of insect behavior, **3**, (1990), 159-168.

Vera Isaevna Sivtseva
North-Eastern Federal University,
Kulakovskiy st, 42,
677000, Yakutsk, Russia
Email address: verasivtseva@gmail.com

Anton Vasilevich Savvin
North-Eastern Federal University,
Kulakovskiy st, 42,
677000, Yakutsk, Russia
Email address: anv.savvin@gmail.com

Vasiliy Vasilevich Grigoriev
North-Eastern Federal University,
Kulakovskiy st, 42,
677000, Yakutsk, Russia
Email address: v.v.grigorev@s-vfu.ru